High-order coupled cluster method study of frustrated and unfrustrated quantum magnets in external magnetic fields

2009 J. Phys.: Condens. Matter 21 406002

(http://iopscience.iop.org/0953-8984/21/40/406002)

J. Phys.: Condens. Matter **21** (2009) 406002 (12pp) doi:10.1088/0953-8984/21/40/406002

High-order coupled cluster method study of frustrated and unfrustrated quantum magnets in external magnetic fields

D J J Farnell[1], R Zinke[2], J Schulenburg[3] and J Richter[2]

[1] Academic Department of Radiation Oncology, Faculty of Medical and Human Science, University of Manchester, c/o The Christie NHS Foundation Trust, Manchester M20 4BX, UK
[2] Institut für Theoretische Physik, Otto-von-Guericke Universität Magdeburg, POB 4120, 39016 Magdeburg, Germany
[3] Universitätsrechenzentrum, Otto-von-Guericke Universität Magdeburg, POB 4120, 39016 Magdeburg, Germany

E-mail: damian.farnell@manchester.ac.uk

Received 11 May 2009, in final form 22 July 2009
Published 8 September 2009
Online at stacks.iop.org/JPhysCM/21/406002

Abstract

We apply the coupled cluster method (CCM) in order to study the ground-state properties of the (unfrustrated) square-lattice and (frustrated) triangular-lattice spin-half Heisenberg antiferromagnets in the presence of external magnetic fields. Approximate methods are difficult to apply to the triangular-lattice antiferromagnet because of frustration, and so, for example, the quantum Monte Carlo (QMC) method suffers from the 'sign problem'. Results for this model in the presence of magnetic field are rarer than those for the square-lattice system. Here we determine and solve the basic CCM equations by using the localized approximation scheme commonly referred to as the 'LSUBm' approximation scheme and we carry out high-order calculations by using intensive computational methods. We calculate the ground-state energy, the uniform susceptibility, the total (lattice) magnetization and the local (sublattice) magnetizations as a function of the magnetic field strength. Our results for the lattice magnetization of the square-lattice case compare well to the results from QMC approaches for all values of the applied external magnetic field. We find a value for the magnetic susceptibility of $\chi = 0.070$ for the square-lattice antiferromagnet, which is also in agreement with the results from other approximate methods (e.g., $\chi = 0.0669$ obtained via the QMC approach). Our estimate for the range of the extent of the $(M/M_s =) \frac{1}{3}$ magnetization plateau for the triangular-lattice antiferromagnet is $1.37 < \lambda < 2.15$, which is in good agreement with results from spin-wave theory ($1.248 < \lambda < 2.145$) and exact diagonalizations ($1.38 < \lambda < 2.16$). Our results therefore support those from exact diagonalizations that indicate that the plateau begins at a higher value of λ than that suggested by spin-wave theory (SWT). The CCM value for the in-plane magnetic susceptibility per site is $\chi = 0.065$, which is below the result of SWT (evaluated to order $1/S$) of $\chi_{\mathrm{SWT}} = 0.0794$. Higher-order calculations are thus suggested for both SWT and CCM LSUBm calculations in order to determine the value of χ for the triangular lattice conclusively.

(Some figures in this article are in colour only in the electronic version)

1. Introduction

Low-dimensional quantum magnets provide a difficult challenge to the theoretical physicist because of their strong quantum fluctuations and their complex dynamics [1, 2]. These effects lead to rich physics that include novel quantum phases, as well as quantum phase transitions between semi-classical magnetically ordered phases and magnetically disordered quantum phases, see, e.g., [3].

An interesting field of research is that of the behaviour of quantum magnetic systems in the presence of external magnetic fields, see, e.g. [4–8]. This topic has become more important by the discovery of exotic parts of the magnetization curve of quantum antiferromagnets, such as plateaux and jumps [4, 7–19] in the lattice magnetization with respect to the externally applied field. Indeed, the presence of these plateaux and jumps may sometimes be linked purely to quantum effects because they are not observed in equivalent classical models at $T = 0$ [14, 20–22]. Clearly, the behaviour of quantum magnetic materials in the presence of external magnetic fields is an important aspect in their subsequent technological exploitation. Several methods such as quantum Monte Carlo method (QMC), field theories, exact diagonalization of finite systems, spin-wave techniques and strong-coupling approximation have been used [4–8] to study these systems. However, each method has its own specific limitations; for instance, the QMC is restricted (essentially) to unfrustrated systems because of the infamous 'sign problem'.

In this paper we focus on the behaviour of quantum antiferromagnets as they react to externally imposed magnetic fields by a method of quantum many-body theory called the coupled cluster method (CCM) [23–32]. The CCM has been used previously in order to treat a wide range of strongly interacting quantum systems. In particular, the CCM is not restricted, in principle, by the spatial dimensionality of the problem or by the presence of competition between bonds, i.e., in frustrated quantum spin systems. A remarkable advance in the accuracy of the method for a localized approximation scheme called the LSUBm scheme has been afforded by the use of 'high-order' CCM via computer-algebraic implementations [26–29]. This computer code developed by Farnell and Schulenburg [33] is very flexible in terms of the range of underlying crystallographic lattice, spin quantum number, and types of Hamiltonian that may be studied. Furthermore, recent advances to this code now allow 'generalized expectation values' (with respect to one-spin and two-spin operators) and (separately) excited-state properties to be evaluated to high orders of approximation. Indeed, we employ the new code for the generalized expectation values to determine the lattice magnetization and individual sublattice magnetizations of quantum antiferromagnets in external magnetic fields.

The relevant Hamiltonian for an antiferromagnet in an external field is defined by

$$H = \sum_{\langle i,j \rangle} \mathbf{s}_i \cdot \mathbf{s}_j - \lambda \sum_i s_i^z, \tag{1}$$

where the index i runs over all lattice sites on the lattice. The expression $\langle i, j \rangle$ indicates a sum over all nearest-neighbour pairs, although each pair is counted once and once only. The strength of the applied external magnetic field is given by λ.

The quantum ground states at $\lambda = 0$ of all of the cases considered here are semi-classically ordered (albeit the classical order is reduced by quantum fluctuations) [2]. Classically, nearest-neighbours align in antiparallel directions for the bipartite antiferromagnets such as the antiferromagnet on the square lattice and at angles of 120° to each other for the Heisenberg antiferromagnet on the (tripartite) triangular lattice at $\lambda = 0$. In the presence of an externally applied magnetic field ($\lambda > 0$), the classical picture indicates that the spins will cant at various angles and that at a 'saturation' value of $\lambda = \lambda_s$ (square: $\lambda_s = 4$; triangle; $\lambda_s = 4.5$) all spins align with the field. The magnetization saturates to a maximum value $M = M_s$ at this point.

However, we remark that the behaviour of quantum spin-half square-lattice antiferromagnet in a magnetic field [4, 7, 34–40] is (essentially) the same as that of the classical model, albeit modified by quantum fluctuations. Second-order (and third-order) spin-wave theory [36–38] thus provides a good approximation to the behaviour of this model. Exact diagonalizations and QMC simulations [7, 39] also provide good results for this case. Very recently, in [39, 40], the field dependence of the low-energy descriptors of this model (i.e., spin stiffness, spin-wave velocity, and magnetic susceptibility) have been investigated using exact diagonalizations and spin-wave theory. A review of the properties of the spin-half square-lattice antiferromagnet is given by [41].

By contrast, the behaviour of the quantum case for spin-half triangular-lattice antiferromagnet [4, 7–11, 15, 42, 43] is much different to that of the classical model. In particular, a magnetization plateau is observed at $M/M_s = \frac{1}{3}$ over a finite region of λ. The range of this plateau has been estimated by spin-wave theory [10, 11] to be given by $1.248 < \lambda < 2.145$, whereas exact diagonalizations [4, 7–9] predict a region given by $1.38 < \lambda < 2.16$. We note that the application of the QMC method (leading to precise results for bipartite lattices) to the case of the triangular is severely limited by the 'sign problem' due to frustration. The available spin-wave and exact-diagonalization data for the triangular lattice seem to be less accurate and complementary results are desirable. Furthermore, recent experimental evidence [19] for the magnetic material Cs_2CuBr_4 suggests that a series of plateaux might exist at values of M/M_s equal to $1/3$, $1/2$, $5/9$ and $2/3$. The authors of this paper suggest that this might be due to unit cells of differing size for the different plateaux, e.g., each having an overall magnetization of $1/2$, and furthermore that theory has thus far only predicted the first of these at $1/3$. However, the treatment of these possible higher plateau is beyond the scope of this paper.

The main goal of our paper is to explain how the CCM can be used to investigate the magnetization process of quantum antiferromagnets and to provide detailed CCM results for the spin-half Heisenberg antiferromagnets on the square and the triangular lattices. The CCM has previously been applied with much success to the subject of quantum magnetic systems at zero temperature. The CCM provides accurate results even in the presence of very strong frustration. In particular, the use of computer-algebraic implementations [26–29] of the CCM for quantum systems of infinite numbers of particles has been found to be very effective with respect to these spin–lattice problems. Here we present a brief description of the CCM formalism and its application via computational methods to the subject of quantum spin models. We then describe the application of the method to the spin-half Heisenberg model

for the square and triangular lattices at zero temperature in the presence of an external magnetic field. We present our results and then discuss the conclusions of this research.

2. The coupled cluster method (CCM)

As the CCM has been discussed extensively elsewhere (see [23–32]), we do not consider the methodology in depth here. In particular, the interested reader should note that the use of computer-algebraic implementations has been considered in [26–29]. However, it is still important to remark here that the exact ket and bra ground-state energy eigenvectors, $|\Psi\rangle$ and $\langle\tilde{\Psi}|$, of a general many-body system described by a Hamiltonian H, are given by

$$H|\Psi\rangle = E_{\rm g}|\Psi\rangle; \qquad \langle\tilde{\Psi}|H = E_{\rm g}\langle\tilde{\Psi}|. \tag{2}$$

The ket and bra states are parametrized within the CCM as follows:

$$\begin{aligned} |\Psi\rangle &= {\rm e}^{S}|\Phi\rangle; \qquad S = \sum_{I\neq 0}\mathcal{S}_I C_I^{+}, \\ \langle\tilde{\Psi}| &= \langle\Phi|\tilde{S}{\rm e}^{-S}; \qquad \tilde{S} = 1 + \sum_{I\neq 0}\tilde{\mathcal{S}}_I C_I^{-}. \end{aligned} \tag{3}$$

One of the most important features of the CCM is that one uses a single model or reference state $|\Phi\rangle$ that is normalized. This, in turn, leads to a normalization condition for the ground-state bra and ket wavefunctions ($\langle\tilde{\Psi}|\Psi\rangle \equiv \langle\Phi|\Phi\rangle = 1$). The model state is required to have the property of being a cyclic vector with respect to two well-defined Abelian subalgebras of *multi-configurational* creation operators $\{C_I^{+}\}$ and their Hermitian-adjoint destruction counterparts $\{C_I^{-} \equiv (C_I^{+})^{\dagger}\}$. For spin systems the model state $|\Phi\rangle$ typically can be chosen as an independent-spin product state and the corresponding operators $\{C_I^{+}\}$ can be expressed as a product of a set of spin lowering operators, see below and for more details also [26–29].

The CCM formalism is exact in the limit of inclusion of all possible multi-spin cluster correlations within S and $\tilde{S}$, although this is usually impossible to achieve practically. It is therefore necessary to utilize various approximation schemes within S and $\tilde{S}$. Here we use the localized LSUBm scheme, in which all multi-spin correlations over distinct locales on the lattice defined by m or fewer contiguous sites are retained. This approximation scheme has been successfully applied to determine the ground-state phases of quantum spin systems, see e.g. [27, 29]. The CCM is a bi-variational formulation in which the bra and ket states are parametrized separately. This means that the ket and bra states are not explicitly constrained to be Hermitian conjugates. However, an advantage of this approach is that the Goldstone linked cluster theorem is obeyed and so results may be found in the infinite-lattice limit $N \to \infty$ from the outset. The important Hellmann–Feynman theorem is also obeyed at all levels of approximation. The ket-state and bra-state equations are obtained using the following formulae,

$$\langle\Phi|C_I^{-}{\rm e}^{-S}H{\rm e}^{S}|\Phi\rangle = 0, \qquad \forall I \neq 0; \tag{4}$$

$$\langle\Phi|\tilde{S}{\rm e}^{-S}[H, C_I^{+}]{\rm e}^{S}|\Phi\rangle = 0, \qquad \forall I \neq 0. \tag{5}$$

The method in which equations (4) and (5) are solved has been discussed extensively elsewhere [23–32]. However, we remark here that the computational method for solution of the CCM problem may be broken into three parts. The first task is, namely, to enumerate the fundamental set of CCM clusters for a given level of approximation. Secondly, we must determine the ket-state equations in terms of the CCM ket-state correlation coefficients by pattern matching those clusters C_I^{-} in the fundamental set to term in ${\rm e}^{-S}H{\rm e}^{S}$. Once we have determined the ket-state equations, the bra-state equations may be determined directly. Finally, we solve the coupled CCM equations for the ket- and bra-state correlation coefficients, e.g., by using the Newton–Raphson method for the ket-state equations. Expectation values such as the lattice magnetization may be obtained after we have solved for both the ket and bra states. Again, we refer the interested reader to [26–29] for more details of the practicalities of carrying out CCM calculations to high order.

Here we use the classical ground states of these systems of the Heisenberg model in an external magnetic field as the model state. However, the magnitude of the characteristic canting angles in the quantum model (i.e., the angle between the local directions of the spins and the external magnetic field) may be different from the corresponding classical value. Hence, we do not choose the classical result for those angles. Indeed, we consider the angles as a free parameters in the CCM calculation, which has to be determined by minimization of the CCM ground-state energy.

The ground state of the classical system at zero external field ($\lambda = 0$) has nearest neighbouring spins aligning in opposite directions for the bipartite lattices (e.g., the square lattice) and at angles of 120° to each other for the triangular lattice. Classically, the spins react to an external magnetic field by changing their alignment to that of the direction of the field. This is shown in figure 1. For the bipartite lattices, the spins thus cant at an angle of θ and $\pi - \theta$ to the x-axis, as is shown in figure 1(a). By contrast, for the tripartite triangular lattice and related frustrated lattices one ought to distinguish between an applied field within the plane defined by the 120° planar state and a field perpendicular to this plane. Although on the classical level both cases are energetically equivalent [10, 20–22], thermal or quantum fluctuations favour the planar configuration [10, 20–22]. Therefore in the present paper we restrict our considerations to planar states and a corresponding magnetic field applied within this plane. Following [10, 15] we employ three different model states for the tripartite triangular lattice. The first such model state is one in which two spins on the A and B sublattices point generally in the direction of the external magnetic field. However, they form angles α and $\pi - \alpha$ to the x-axis, as shown in the model state I of figure 1(b). The remaining spins on the C sublattice point in a direction antiparallel to the applied external field. The second model state II of figure 1(c) for the triangular lattice has two spins on the A and B sublattices that align completely with the external magnetic field and the remaining spins that align antiparallel to the external magnetic field. The final model state III has two spins on the A and B sublattices

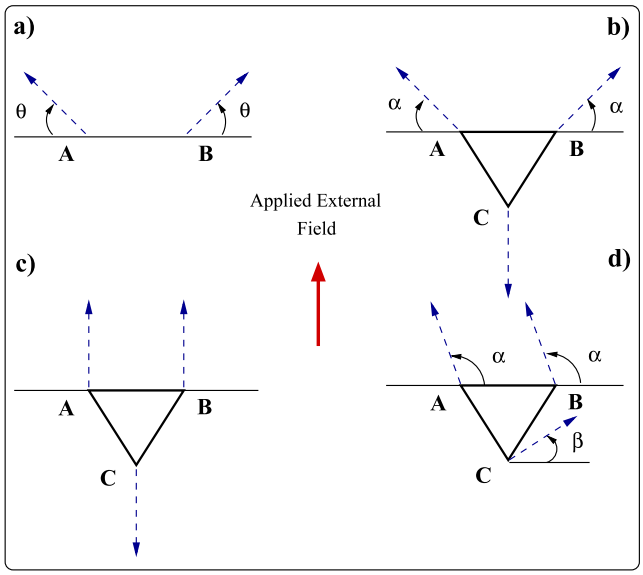

Figure 1. The model states used in the CCM calculations for the Heisenberg model in an external magnetic field. (a) The bipartite lattices. Spins on the A and B sublattices make angles θ to the x-axis. (b) The first model state for the triangular lattice (model state I). Spins on the A and B sublattices make angles α to the x-axis. Spins on the C sublattice point downwards. (c) The second model state for the triangular lattice (model state II). Spins on the A and B sublattices point upwards. Spins on the C sublattice point downwards. (d) The third model state for the triangular lattice (model state III). Spins on the A and B sublattices make angles α to the x-axis. Spins on the C make an angle β to the x-axis. (Model state II is also a limiting case of model states I and III.)

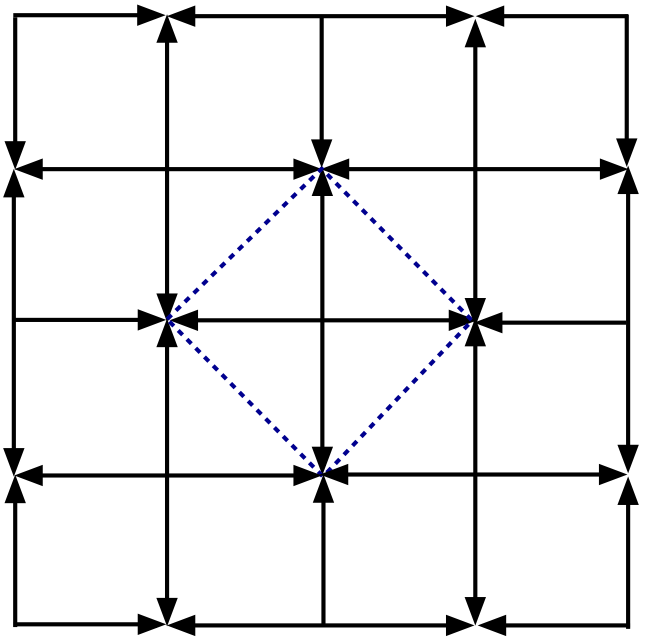

Figure 2. The bond directionality of the Heisenberg Hamiltonian after rotation of the local coordinate axes in the spin space. The directions of the bonds are indicated by the arrows placed on the square lattice. The two-site unit cell is also shown in dotted lines.

that form an angle α to the x-axis and another spin on the C sublattice that forms a (initially negative) angle of β to the x-axis, as is also shown in figure 1(d). Model state II is clearly a limiting case of both model states, I and III. (For example, we obtain model state II from model state III by setting $\alpha = \pi/2$ and $\beta = -\pi/2$.)

In order to simplify the problem, we now rotate the local coordinate axes in the spin space so that all spins appear notationally to point in the downwards z-direction. For a spin making an angle of θ to the x-axis, the rotation of the local axes is given by,

$$\begin{aligned} s^x &\rightarrow -s^x\sin(\theta) + s^z\cos(\theta), \qquad s^y \rightarrow s^y \\ s^z &\rightarrow -s^x\cos(\theta) - s^z\sin(\theta). \end{aligned} \tag{6}$$

The spins in the model state $|\Phi\rangle$ now all appear to point downwards, i.e. $|\Phi\rangle = |\cdots\downarrow\downarrow\downarrow\downarrow\cdots\rangle$. The corresponding creation $\{C_I^+\}$ are then given by $\{C_I^+\} = s_i^+, s_i^+s_j^+, s_i^+s_j^+s_k^+, \ldots$, where the indices $i, j, k, \ldots$ denote arbitrary lattice sites. Furthermore, the Hamiltonian for the bipartite lattices in the rotated coordinate frame (i.e., with spins on the A sublattice making an angle θ to the negative x-axis and spins on the B sublattice making an angle θ to the positive x-axis as shown in figure 1) is now given by

$$\begin{aligned} H = \sum_{\langle i\rightarrow j\rangle} \{ & -\tfrac{1}{4}(1+\cos(2\theta))(s_i^+s_j^+ + s_i^-s_j^-) \\ & + \tfrac{1}{4}(1-\cos(2\theta))(s_i^+s_j^- + s_i^-s_j^+) \\ & - \cos(2\theta)s_i^zs_j^z + \tfrac{1}{2}\sin(2\theta)(s_i^zs_j^+ + s_i^zs_j^-) \\ & - \tfrac{1}{2}\sin(2\theta)(s_i^+s_j^z + s_i^-s_j^z)\} \\ & + \lambda\sin(\theta)\sum_i s_i^z - \frac{\lambda}{2}\cos(\theta)\sum_{i_\mathrm{A}}(s_{i_\mathrm{A}}^+ + s_{i_\mathrm{A}}^-) \\ & + \frac{\lambda}{2}\cos(\theta)\sum_{i_\mathrm{B}}(s_{i_\mathrm{B}}^+ + s_{i_\mathrm{B}}^-). \end{aligned} \tag{7}$$

We note that the sign in equation (7) for those terms for s^zs^+ and s^zs^- for a bond going from i to j has an opposite sign for those same terms for a bond going from j to i. This is called a 'bond directionality' and is indicated in the above equation by the arrow in the symbol $\langle i \rightarrow j\rangle$. An illustrative example of bond directionality in the Hamiltonian for the square-lattice case is shown in figure 2. We note also that i_A runs over all A sublattice sites, i_B runs over all B sublattice sites, and i runs over all lattice sites. The translational symmetry of equation (7) compared to the original problem has also been reduced. We must include two sites in the unit cell, as is also shown in figure 2.

Similar calculations may be carried out for the triangular lattice. We have three new Hamiltonians after rotation of the local spin axes of the spins for all three model states I, II, and III in figures 1(b)–(d) for the triangular lattice case such that all spins again appear to point downwards. The Hamiltonian for model state I, figure 1(b), for the triangular lattice is:

$$\begin{aligned} H = \sum_{\langle i_\mathrm{A}\rightarrow i_\mathrm{B}\rangle} \{ & -\tfrac{1}{4}(1+\cos(2\alpha))(s_{i_\mathrm{A}}^+s_{i_\mathrm{B}}^+ + s_{i_\mathrm{A}}^-s_{i_\mathrm{B}}^-) \\ & + \tfrac{1}{4}(1-\cos(2\alpha))(s_{i_\mathrm{A}}^+s_{i_\mathrm{B}}^- + s_{i_\mathrm{A}}^-s_{i_\mathrm{B}}^+) \\ & - \cos(2\alpha)s_{i_\mathrm{A}}^zs_{i_\mathrm{B}}^z + \tfrac{1}{2}\sin(2\alpha)(s_{i_\mathrm{A}}^zs_{i_\mathrm{B}}^+ + s_{i_\mathrm{A}}^zs_{i_\mathrm{B}}^-) \end{aligned}$$

$$
\begin{aligned}
&- \tfrac{1}{2}\sin(2\alpha)(s^{+}_{i_{\rm A}}s^{z}_{i_{\rm B}} + s^{-}_{i_{\rm A}}s^{z}_{i_{\rm B}})\} \\
&+ \sum_{\langle i_{\rm B,C}\rightarrow i_{\rm C,A}\rangle}\{-\tfrac{1}{4}(1+\sin(\alpha))(s^{+}_{i_{\rm B,C}}s^{+}_{i_{\rm C,A}} + s^{-}_{i_{\rm B,C}}s^{-}_{i_{\rm C,A}}) \\
&+ \tfrac{1}{4}(1-\sin(\alpha))(s^{+}_{i_{\rm B,C}}s^{-}_{i_{\rm C,A}} + s^{-}_{i_{\rm B,C}}s^{+}_{i_{\rm C,A}}) \\
&- \sin(\alpha)s^{z}_{i_{\rm B,C}}s^{z}_{i_{\rm C,A}} + \tfrac{1}{2}\cos(\alpha)(s^{z}_{i_{\rm B,C}}s^{+}_{i_{\rm C,A}} + s^{z}_{i_{\rm B,C}}s^{-}_{i_{\rm C,A}}) \\
&- \tfrac{1}{2}\cos(\alpha)(s^{+}_{i_{\rm B,C}}s^{z}_{i_{\rm C,A}} + s^{-}_{i_{\rm B,C}}s^{z}_{i_{\rm C,A}})\} \\
&- \lambda\sum_{i_{\rm C}}s^{z}_{i_{\rm C}} + \lambda\sin(\alpha)\left(\sum_{i_{\rm A}}s^{z}_{i_{\rm A}} + \sum_{i_{\rm B}}s^{z}_{i_{\rm B}}\right) \\
&- \frac{\lambda}{2}\cos(\alpha)\sum_{i_{\rm A}}(s^{+}_{i_{\rm A}} + s^{-}_{i_{\rm A}}) + \frac{\lambda}{2}\cos(\alpha)\sum_{i_{\rm B}}(s^{+}_{i_{\rm B}} + s^{-}_{i_{\rm B}}), \quad (8)
\end{aligned}
$$

where the sum $\langle i_{\rm A}\rightarrow i_{\rm B}\rangle$ goes from sublattice A to sublattice B (and with directionality). Note that $\langle i_{\rm B,C}\rightarrow i_{\rm C,A}\rangle$ indicates a sum that goes from sublattice B to sublattice C and sublattice C to sublattice A, respectively (and with directionality). A similar treatment may be carried out for the model state III, figure 1(d). Hence, if those spins on the A and B sublattices make an angle α to the x-axis and those spins on the C sublattice make an angle β to the x-axis and employing the rotation of the local spin axes of equation (6), we find that,

$$
\begin{aligned}
H = &\sum_{\langle i_{\rm C}\rightarrow i_{\rm A,B}\rangle}\{\tfrac{1}{4}(-1+\cos(\alpha-\beta))(s^{+}_{i_{\rm C}}s^{+}_{i_{\rm A,B}} + s^{-}_{i_{\rm C}}s^{-}_{i_{\rm A,B}}) \\
&+ \tfrac{1}{4}(1+\cos(\alpha-\beta))(s^{+}_{i_{\rm C}}s^{-}_{i_{\rm A,B}} + s^{-}_{i_{\rm C}}s^{+}_{i_{\rm A,B}}) \\
&+ \cos(\alpha-\beta)s^{z}_{i_{\rm C}}s^{z}_{i_{\rm A,B}} \\
&+ \tfrac{1}{2}\sin(\alpha-\beta)(s^{+}_{i_{\rm C}}s^{z}_{i_{\rm A,B}} + s^{-}_{i_{\rm C}}s^{z}_{i_{\rm A,B}}) \\
&- \tfrac{1}{2}\sin(\alpha-\beta)(s^{z}_{i_{\rm C}}s^{+}_{i_{\rm A,B}} + s^{z}_{i_{\rm C}}s^{-}_{i_{\rm A,B}})\} \\
&+ \sum_{\langle i_{\rm A},i_{\rm B}\rangle}\{\tfrac{1}{2}(s^{+}_{i_{\rm A}}s^{-}_{i_{\rm B}} + s^{-}_{i_{\rm A}}s^{+}_{i_{\rm B}}) + s^{z}_{i_{\rm A}}s^{z}_{i_{\rm B}}\} \\
&+ \lambda\sin(\alpha)\left(\sum_{i_{\rm A}}s^{z}_{i_{\rm A}} + \sum_{i_{\rm B}}s^{z}_{i_{\rm B}}\right) + \lambda\sin(\beta)\sum_{i_{\rm C}}s^{z}_{i_{\rm C}} \\
&+ \frac{\lambda}{2}\cos(\alpha)\left\{\sum_{i_{\rm A}}(s^{+}_{i_{\rm A}} + s^{-}_{i_{\rm A}}) + \sum_{i_{\rm B}}(s^{+}_{i_{\rm B}} + s^{-}_{i_{\rm B}})\right\} \\
&+ \frac{\lambda}{2}\cos(\beta)\sum_{i_{\rm C}}(s^{+}_{i_{\rm C}} + s^{-}_{i_{\rm C}}), \quad (9)
\end{aligned}
$$

where the sum $\langle i_{\rm C}\rightarrow i_{\rm A,B}\rangle$ goes from sublattice C to sublattices A and B (with directionality) and $\langle i_{\rm A}, i_{\rm B}\rangle$ goes over each bond connecting the A and B sublattices, but counting each one once only (and without directionality). We note that we have three sites in the unit cell for all of the models states used for the triangular lattice antiferromagnet.

Note that in addition to the model states presented above, spin liquids such as valence-bond crystal states may be treated via the CCM is by using a dimerized or plaquette (etc) as relevant model state. A corresponding matrix algebra [25] is then used with respect to this state. However, a simpler approach is now also available that relies on finding special solutions of the CCM equations for the Néel-type model states used here [32]. These allow us to treat via existing high-order formalism and computer code, for example, spontaneous symmetry breaking in the spin-half one-dimensional J_1–J_2 (Majumdar–Ghosh) model [32]. The CCM is thus not restricted purely to semi-classical systems.

We consider the angles as free parameters in the CCM calculation. They are determined by direct minimization of the CCM ground-state energy. This was achieved computationally at a given level of LSUBm approximation, and a minimum ground-state energy with respect to these canting angles was also found computationally for a given fixed value of λ. There was only one angle for the square-lattice antiferromagnet (and for model state I for the triangular lattice) and there were two such angles for model state III for the triangular lattice. The next value of λ was then determined incrementally and the minimization process of the energy with respect to the canting angles repeated. The fact that we had to minimize the ground-state energy with respect to such angles at each value of λ made the CCM calculations much more costly in terms of computing time required than the equivalent situations at zero external magnetic field, which requires no such minimization. Furthermore, we see that the Hamiltonians of equations (7)–(9) do not conserve the quantity $s^{z}_{T} \equiv \sum_{i} s^{z}_{i} = 0$, which is preserved for the square-lattice antiferromagnet at $\lambda = 0$. For these reasons, CCM calculations in the presence of external magnetic fields are more challenging than their zero-field counterparts.

A final point is that the inclusion of the CCM SUB1 terms of form $S_1 \equiv \mathcal{S}_{i_1}s^{+}_{i}$ in the ground ket and bra states is also equivalent to a rotation of the local spin axes [23]. For example, for the spin-half system, we note that $(s^{+}_{i})^2|\Phi\rangle = 0$ and so we can prove that $e^{S_1}|\Phi\rangle = \Pi_i(1+\mathcal{S}_{i_1}s^{+}_{i})|\Phi\rangle$. This produces a mixture of 'up' and 'down' spins at each site, which may be thought of (as may be seen from equation (6) above, for example) as the same as a rotation of local spin axes. Hence, we conclude that SUB1 is equivalent to a rotation of the axes. Previous calculations for Heisenberg antiferromagnets in external magnetic fields [23] made the explicit assumption that the correlation coefficients of the SUB1 terms may be set to zero, and we make the same explicit assumption here. We minimize the ground-state energy explicitly with respect to the angles in our model state. Note that we go to much higher orders of LSUBm approximation than those calculations presented in [23].

To investigate the magnetization process in antiferromagnets we have to consider the total lattice magnetization M along the direction of the magnetic field. This quantity (in the initial coordinate frame prior to rotation of the local spin axes) is defined by $M = \frac{1}{Ns}\langle\sum_i s^{z}_{i}\rangle = \frac{1}{Ns}\langle\tilde{\Psi}|\sum_i s^{z}_{i}|\Psi\rangle$ (s is the spin quantum number which is $s = 1/2$ throughout this paper). In the rotated coordinate frame (and in which all of the spins point appear 'mathematically' to downwards), the lattice magnetization for the bipartite lattices is now given by

$$
\begin{aligned}
M = &-\frac{\sin(\theta)}{Ns}\sum_{i}\langle\tilde{\Psi}|s^{z}_{i}|\Psi\rangle - \frac{\cos(\theta)}{2Ns}\sum_{i_{\rm A}}\langle\tilde{\Psi}|s^{+}_{i_{\rm A}} + s^{-}_{i_{\rm A}}|\Psi\rangle \\
&+ \frac{\cos(\theta)}{2Ns}\sum_{i_{\rm B}}\langle\tilde{\Psi}|s^{+}_{i_{\rm B}} + s^{-}_{i_{\rm B}}|\Psi\rangle, \quad (10)
\end{aligned}
$$

where, again, $i_{\rm A}$ runs over all A sublattice sites, $i_{\rm B}$ runs over all B sublattice sites, and i runs over all lattice sites. We are able to determine readily the lattice magnetization once the ket- and bra-state equations have been solved for a given value of λ. Furthermore, similar expressions to equation (10) may be

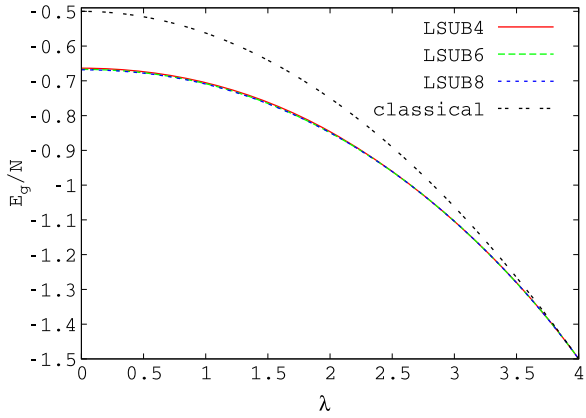

Figure 3. Results for the ground-state energy per site E_g/N of the spin-half square-lattice Heisenberg antiferromagnet in dependence on an external magnetic field of strength λ. Note that the curves for LSUB4, LSUB6, LSUB8 almost coincide.

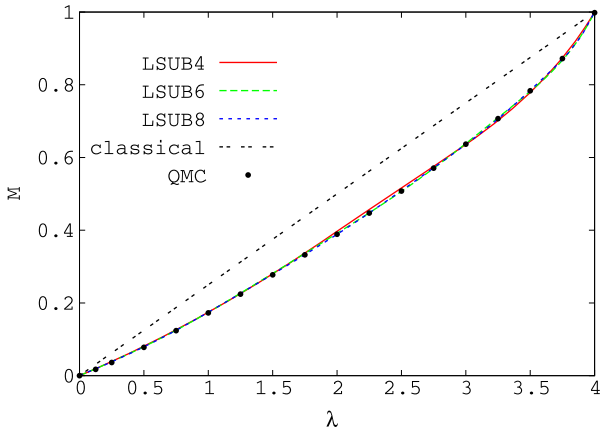

Figure 4. Results for the total lattice magnetization M of the spin-half square-lattice Heisenberg antiferromagnet in the presence of an external magnetic field of strength λ compared to results of QMC [7]. Note that the curves for LSUB4, LSUB6, LSUB8 almost coincide.

obtained for the lattice magnetization for the triangular lattice for model states I, II, III, figures 1(b)–(d). We note that the magnetization found on the three sublattices may become non-equivalent in a magnetic field for the triangular-lattice case. Indeed, for the triangular lattice, the expression for the lattice magnetization aligned in the direction of the applied magnetic field on the individual sublattices (denoted, M_A, M_B, and M_C) in terms of the global axes prior to rotation of the local spin axes is given by

$$M_{A,B,C} = \frac{1}{N_{A,B,C}\, s} \sum_{i_{A,B,C}} \langle \tilde{\Psi} | s^z_{i_{A,B,C}} | \Psi \rangle, \qquad (11)$$

where the index i_A runs over all N_A sites on sublattice A, the index i_B runs over all N_B sites on sublattice B, and the index i_C runs over all N_C sites on sublattice C. Clearly, we see that $N = N_A + N_B + N_C$ and that $M = (M_A + M_B + M_C)/3$.

3. Results

Now we present and discuss the results for the two models under consideration calculated by the CCM as illustrated above. We start with the spin-half square-lattice Heisenberg antiferromagnet. The ground-state energy in dependence of this model is shown in figure 3. The CCM results converge rapidly with increasing LSUBm level of approximation. As seen in previous CCM calculations [27], the ground-state energy in the limit of vanishing external field ($\lambda = 0$) is approximated well. The interested reader is referred to [27] for a more detailed discussion of these results. We also find that the exact result for the saturation field $M = M_s$ at $\lambda_s = 4$ is also reproduced. At this point the spins all lie in the direction of the external field.

The results for the lattice magnetization are shown in figure 4. There is a considerable difference between the results for the spin-half quantum model and the classical straight-line behaviour (i.e., $M_{\text{Classical}} = \frac{1}{4}\lambda$). Clearly, this difference is because of quantum effects. It is also obvious from figure 4 that the magnetization of the quantum model is below that

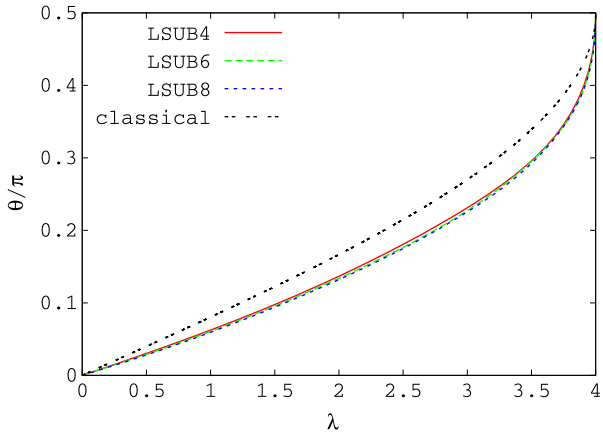

Figure 5. Results for the canting angle θ/π obtained for the model state for the spin-half square-lattice Heisenberg antiferromagnet (see figure 1(a)) in the presence of an external magnetic field of strength λ. Note that the curves for LSUB4, LSUB6, LSUB8 almost coincide.

of the classical magnetization in the region $0 < \lambda < \lambda_s$. Again we note that the LSUBm results appear to converge with increasing m for all values of λ. For example, the difference between the LSUB6 and LSUB8 results for the lattice magnetization is less than 2×10^{-3} for all values of λ, and it is impossible to be detected by eye in figure 4. From figure 4 it is also evident that the CCM results for the lattice magnetization are in excellent agreement with the results of QMC [7], which can be considered as the most accurate results available.

In addition to the energy and the magnetization we can also present results for the canting angle θ (cf figure 1) of the quantum model, see figure 5. Again, there is a noticeable difference between the values for the classical and the quantum angle. This difference first increases with λ up to about $\lambda \approx 3.5$. Beyond $\lambda \approx 3.5$ the quantum angle very rapidly approaches the saturation value $\theta_s = \pi/2$.

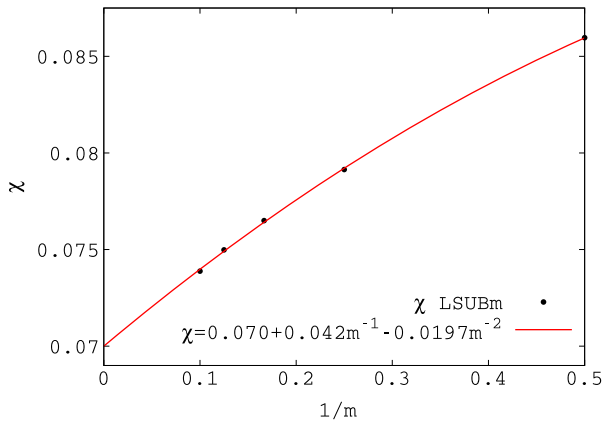

Figure 6. LSUBm results for the zero-field uniform susceptibility $\chi(\lambda \to 0)$ for the spin-half square-lattice Heisenberg antiferromagnet (see figure 1(a)) with $m = \{2, 4, 6, 8, 10\}$ and the polynomial fit according to $\chi(m) = c_0 + c_1/m + c_2/m^2$.

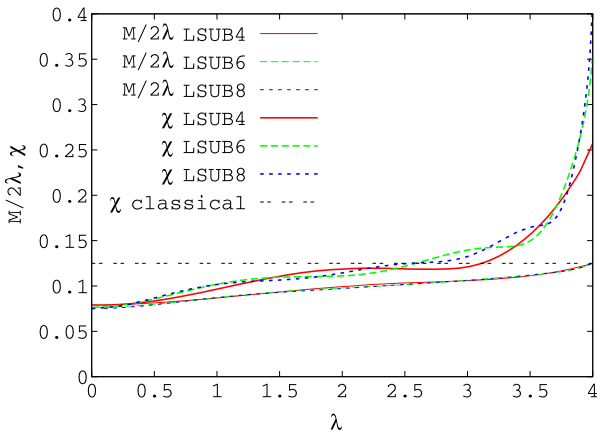

Figure 7. Susceptibility χ, see equation (12), and the quotient $M/2\lambda$ in dependence on the magnetic field λ the for the spin-half square-lattice Heisenberg antiferromagnet. Note that the $M/2\lambda$ curves for LSUB4, LSUB6, LSUB8 almost coincide.

In the next step the CCM results for the ground-state energy and the lattice magnetization in dependence on magnetic field can be used to calculate the uniform magnetic susceptibility, given by

$$\chi \equiv \frac{1}{2}\frac{\mathrm{d}M}{\mathrm{d}\lambda} = -\frac{1}{N}\frac{\mathrm{d}^2 E_\mathrm{g}}{\mathrm{d}\lambda^2}. \tag{12}$$

Note that factor of $\frac{1}{2}$ in $\frac{1}{2}\frac{\mathrm{d}M}{\mathrm{d}\lambda}$ is due to definition of M in the interval $[0, 1]$. Note further that we consider here χ as susceptibility per site[4]. For the concrete calculation of χ we have used the second derivative of the energy. To check the accuracy for low fields we have also determined χ numerically via direct determination from M by using $\frac{\mathrm{d}M}{\mathrm{d}\lambda}$. We found that $\frac{1}{2}\frac{\mathrm{d}M}{\mathrm{d}\lambda}$ and $\frac{1}{N}\frac{\mathrm{d}^2 E_\mathrm{g}}{\mathrm{d}\lambda^2}$ agree to at least six decimal places of precision.

The zero-field uniform susceptibility $\chi(\lambda \to 0)$, the ground-state energy, the sublattice magnetization, the spin stiffness, and the spin-wave velocity constitute the fundamental parameter set that determines the low-energy physics of magnetic systems. The results for the ground-state energy, the sublattice magnetization, the spin stiffness for the square-lattice Heisenberg antiferromagnet at $\lambda = 0$ have been calculated by the CCM previously. The interested reader is referred to [27, 30, 31] for more details. However, CCM results for the susceptibility χ were not determined by these earlier calculations. Here we find that $\chi = 0.085\,96, 0.079\,15, 0.076\,50, 0.074\,98$, and $0.073\,88$ for the LSUB2, LSUB4, LSUB6, LSUB8, and LSUB10 approximations, respectively. Since the LSUBm approximation becomes exact for $m \to \infty$, it is useful to extrapolate the 'raw' LSUBm data to $m \to \infty$. Meanwhile there is much empirical experience how to extrapolate CCM LSUBm data for physical quantities such as the spin stiffness [30, 31] and 'generalized' susceptibilities [31] which are also related to a second derivative of the ground energy E_g. Hence, we use the same extrapolation rule for the zero-field uniform susceptibility that has previously been found to give good results for the spin stiffness and also for 'generalized' susceptibilities [30, 31] given by $\chi(m) = c_0 + c_1/m + c_2/m^2$. We see from figure 6 that this rule provides a good method of extrapolation of our data. The corresponding extrapolation then yields values for the susceptibility of $\chi = 0.0700(6)$. (The number in brackets indicate the standard deviation.) This result is in reasonable agreement with data obtained by other methods, e.g. QMC ($\chi = 0.0669(7)$) [35], series expansion ($\chi = 0.0659(10)$) [36], linear spin-wave theory ($\chi = 0.056\,11$) [34], second-order spin-wave theory ($\chi = 0.064\,26$) [38], and third-order spin-wave theory ($\chi = 0.062\,91$) [37].

The field dependence of χ is also of experimental interest, see e.g. [18, 44–46]. We present LSUB4, LSUB6, and LSUB8 data for the field dependence of χ in figure 7. We note that the magnetization divided by the applied external field is often considered in experimental studies. Hence, results for $M/2\lambda$ are given also in figure 7. For the sake of comparison, the classical value $\chi_\mathrm{clas} = 1/8$ is also shown in this figure and we remark that this value is clearly independent of λ. From figure 7 it is obvious that χ and $M/2\lambda$ agree well with each other up to about $\lambda = 0.4 = \lambda_\mathrm{s}/10$. The difference between results of the LSUB8 approximation and the classical result is about 4% at $\lambda = 0.4$. However, these two sets of results begin to deviate significantly for larger λ. Hence, the quantity $M/2\lambda$ is a good approximation for χ for magnetic fields used in real experiments for systems with large saturation fields λ_s, and *not* for systems with low λ_s. We observe that χ increases with λ as we move away from the zero-field point, $\lambda = 0$. Similar increases in χ with the external field have been observed experimentally, e.g., for the quasi-two-dimensional antiferromagnet $Ba_2CuGe_2O_7$ [44]. Moreover, these results are in agreement with recent results obtained by exact diagonalizations, QMC simulations, and spin-wave theory [39, 40]. As seen for these other methods, the susceptibility is near the constant classical value for magnetic fields $1.5 \lesssim \lambda \lesssim 3.5$, although it starts rapidly to increase approaching the saturation field. Finally, weak oscillations

[4] χ is sometimes defined per volume, see e.g. [42]. Although this factor is unity for the square lattice, it yields a different factor of $2/\sqrt{3}$ for the triangular lattice.

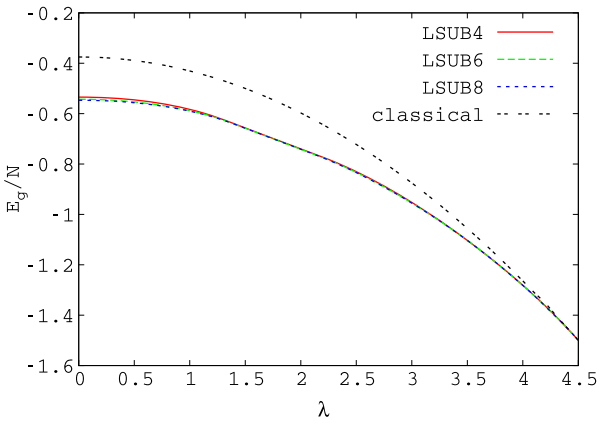

Figure 8. Results for the ground-state energy per site E_g/N of the spin-half triangular-lattice Heisenberg antiferromagnet in the presence of an external magnetic field of strength λ. Note that the results for LSUB4, LSUB6, LSUB8 are clearly converging rapidly for all values of λ.

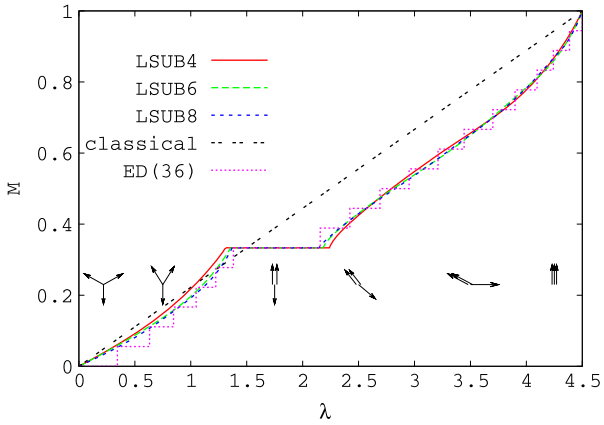

Figure 9. Results for the total lattice magnetization M of the spin-half triangular-lattice Heisenberg antiferromagnet in the presence of an external magnetic field of strength λ. CCM results are compared to those results of exact diagonalizations [7]. The arrows illustrate the actual spin directions. We use model state I for $\lambda \leqslant \lambda_1$ and we use model state III for $\lambda \geqslant \lambda_2$ (see figure 1). Both model states give identical results within the plateau $\lambda_1 \leqslant \lambda \leqslant \lambda_2$.

are seen for $1.5 \lesssim \lambda \lesssim 3.5$, although these are believed to be artefacts of CCM LSUBm approximation. We note that the number of oscillations increases are we increase the LSUBm approximation level, although their amplitude decreases markedly. In the limit, $m \to \infty$, it is expected that these oscillations will disappear entirely.

We conclude from all of these results that the CCM provides precise results for the behaviour of the spin-half square-lattice quantum antiferromagnet in an external magnetic field. However, we see also from these results that the classical picture is essentially correct. Quantum mechanical effects modify, but do not change, the essential physics that occur in this unfrustrated quantum spin system.

We now consider the spin-half antiferromagnet on the triangular lattice. However, the situation is more complicated here because we have three sublattices in this case. As discussed above, we employ therefore the model states I, II, III shown in figures 1(b)–(d). The computational effort of the CCM calculations presented here for the model state III to very high orders is very great because we also need to find the minimum of the energy with respect to two canting angles, namely α and β. The CCM calculation for the model state III in LSUB8 approximation was performed on a Beowulf cluster using 110 cores (Intel XEON 3 GHz CPU). On this computer the running time for one data point was approximately 2 days. The CCM has been shown to be fully competitive with the results of other methods at the levels of approximation currently available to use using parallel computer methods (currently: a maximum of 1000 CPUs in parallel). The interested reader is referred, e.g., to [26–31] for detailed comparisons of CCM results to the best of other methods.

The results for the ground-state energy are shown in figure 8. We note that the results for the model state with lowest energy are shown only as a function of λ in figure 8. Thus, results of model state I only are presented for small values of the applied magnetic field strength λ and results of model state III only are presented for higher values of λ near to λ_s. The results of both model states coincide in the intermediate regime. Again, these LSUBm series of results are found to converge rapidly with increasingly levels of LSUBm approximation over all values of the external field parameter λ. As may also be observed in figure 8, there is also a large reduction in the ground-state energy of the CCM results compared to the classical results for the energy (except in the trivial limit $\lambda \to \lambda_s = 4.5$).

The results for the total lattice magnetization are shown in figure 9. The LSUBm results are again seen to converge rapidly for increasing m. However, there is a radical departure from the classical straight-line behaviour (i.e. $M_{\text{Classical}} = \frac{2}{9}\lambda$) in this case. Thus, we find that the quantum model deviates from the linear relationship between M and λ. The most prominent feature of our CCM results is the plateau in the M versus λ curve at $M/M_s = \frac{1}{3}$. Note that the plateau corresponds to the 'straight' part of the curve in the $E_g(\lambda)$ curve shown in figure 8. Note further that this plateau is well known and has been found by other approximate methods [4, 7–10, 15]. The ground state of the quantum system over the finite, non-zero range of λ for the plateau region has ordering of the form shown in model state II of figure 1(c). Importantly, this is an example of when quantum fluctuations favour collinear ordering (so called 'order from disorder' phenomenon, see e.g. [47–49]). This plateau state of model state II is observed only at a single point classically, namely, at $\lambda = 1.5$. The classical ground state is given by model state II in figure 1(c) only at this point, see also [20–22]. Indeed, states I, II and III are equivalent classically at the point $\lambda = 1.5$. The values for the starting (λ_1) and the end point (λ_2) of the plateau state calculated within different LSUBm approximations are shown in table 1. The most accurate values are provided by the LSUB8 approximation, namely, that $\lambda_1 \approx 1.37$ and $\lambda_2 \approx 2.15$. These results may therefore serve as the CCM estimate for the plateau width. We note that the results for λ_1 and λ_2 for even and odd values of m ought to converge to the

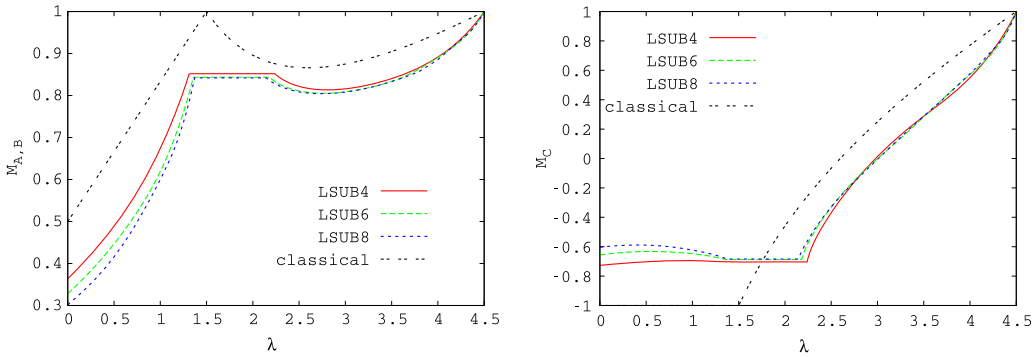

Figure 10. Results for the sublattice magnetization M_γ ($\gamma = \{\mathrm{A}, \mathrm{B}, \mathrm{C}\}$) on individual sublattices A and B (left) and C (right) of the spin-half triangular-lattice Heisenberg antiferromagnet in the presence of an external magnetic field of strength λ. (Note that $M_\mathrm{A} = M_\mathrm{B}$ for all λ.)

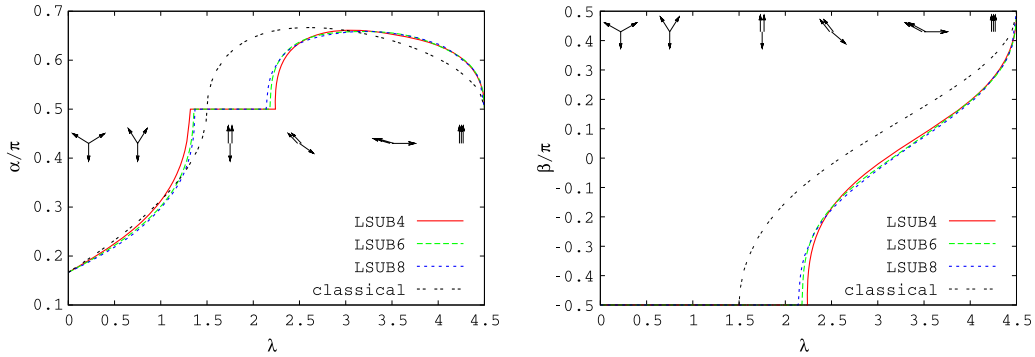

Figure 11. Results for the angle α/π (left) and β/π (right) in the model state for the spin-half triangular-lattice Heisenberg antiferromagnet in the presence of an external magnetic field of strength λ. The arrows illustrate the actual spin directions.

same values in this limit. Our estimate for the range of the plateau is in also reasonable agreement with those results of spin-wave theory [10] and exact diagonalizations [7], which both predict a similar width for the plateau with respect to the applied external magnetic field. However, we note that spin-wave theory was carried out only to order $1/S$ for the triangular lattice antiferromagnet in an external field. We believe that higher orders than $1/S$ for spin-wave theory would provide better correspondence to those results of ED and CCM results cited here regarding the range of the plateau. The phenomenon of 'order from disorder' in which quantum fluctuations tend to favour colinear states has studied extensively elsewhere, e.g., [47, 48]. We note that the plateau state (uud) is colinear in the present case, and so our results are another example of this phenomenon. We have shown here that quantum fluctuations stabilize the (uud) state over other states that classically would have had lower energy in the plateau region.

We are able also to calculate the (sub)lattice magnetization (i.e., with respect to the z-direction in the original unrotated spin axes) for the individual sublattices, namely, M_A, M_B and M_C given by equation (11), by using the CCM and as a function of λ. As far as we are aware, these quantities have never before been presented for this model. The results for M_A, M_B and M_C are now presented in figure 10. Once again, we see a radical shift in the quantum solution from the classical result. Interestingly, M_C appears to decrease before approaching the plateau at $\lambda = \lambda_1$, while $M_\mathrm{A} = M_\mathrm{B}$ increase monotonically with λ up to λ_1. On the other hand, $M_\mathrm{A}, M_\mathrm{B}$ decrease with magnetic field in the region $\lambda_2 < \lambda \lesssim 2.8$ above the plateau, while M_C increases monotonically with λ up to λ_s.

Table 1. CCM results for the width of the magnetization plateau for the spin-half Heisenberg antiferromagnet on the triangular lattice.

	λ_1	λ_2
LSUB4	1.312	2.241
LSUB5	1.370	2.030
LSUB6	1.357	2.185
LSUB7	1.375	2.105
LSUB8	1.370	2.145
SWT [10]	1.248	2.145
Exact diagonalizations [7]	1.38	2.16

We discuss next the canting angles α and β in the model states I, II, III (see figures 1(a)–(c)) shown in figure 11. Note again that to the best of our knowledge data for the angles have not been presented previously by other authors. A strong difference between the results of the classical system and those results of the quantum system is again obvious, in particular, in the plateau region where in the quantum model α and β are constant but both angles change rapidly for the classical model. We see that the results for both α and β vary continuously, although not smoothly, for all values of λ. There is no sudden discontinuity in the solution for the angles as was reported, e.g., for spiral phases of some frustrated quantum spin models. Note that above the plateau the angle α does

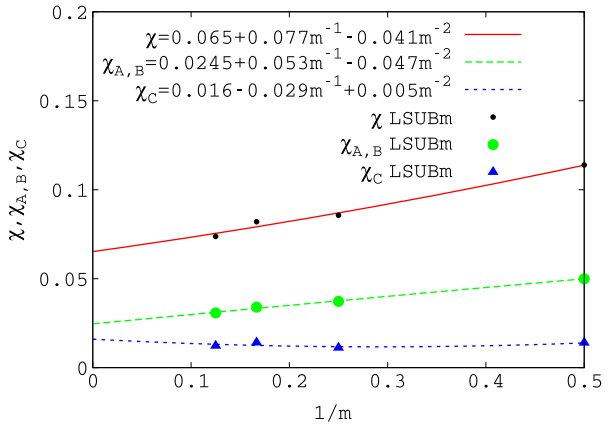

Figure 12. LSUBm results for the zero-field uniform susceptibilities $\chi(\lambda \to 0)$ for the spin-half triangular-lattice Heisenberg antiferromagnet with $m = \{2, 4, 6, 8\}$ and the polynomial fit according to $\chi(m) = c_0 + c_1/m + c_2/m^2$.

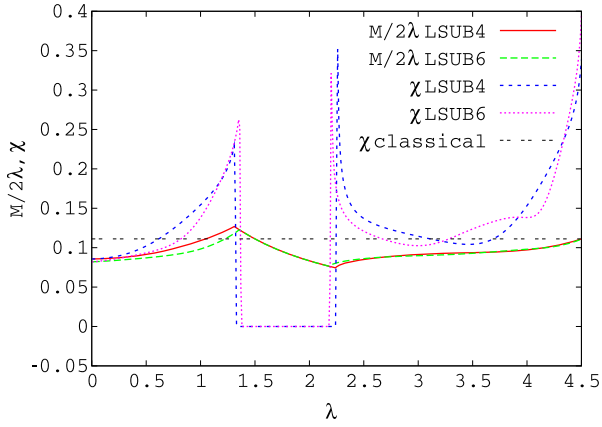

Figure 13. Susceptibility χ, see equation (12), and the quotient $M/2\lambda$ in dependence on the magnetic field λ the for the spin-half triangular-lattice Heisenberg antiferromagnet.

not vary monotonously with field. Rather it first increases to $\alpha > \pi/2$ reaching at maximum at about $\lambda \sim 3.2$. Approaching the saturation then α rapidly decreases to $\alpha = \pi/2$. As far as we aware, no such equivalent experimental results exist for the sublattice magnetizations or tilting angles. We recommend therefore that experimental investigations of these aspects of the magnetization with external field also be carried out.

For the zero-field uniform susceptibility $\chi(\lambda \to 0)$, see equation (12), we obtain $\chi = 0.113\,88$, $0.085\,68$, $0.082\,00$, and $0.073\,78$ for the LSUBm approximation with $m = 2, 4, 6$, and 8. In addition, we can also calculate the individual response of the sublattices on the magnetic field, i.e. $\chi_{\mathrm{A,B,C}} = \frac{1}{6}\frac{\mathrm{d}M_{\mathrm{A,B,C}}}{\mathrm{d}\lambda}$. Due to the relation $M = (M_{\mathrm{A}} + M_{\mathrm{B}} + M_{\mathrm{C}})/3$ we have $\chi = \chi_{\mathrm{A}} + \chi_{\mathrm{B}} + \chi_{\mathrm{C}}$. Again we can extrapolate the data for the susceptibilities to $m \to \infty$ using $\chi(m) = c_0 + c_1/m + c_2/m^2$. The corresponding extrapolation then yields $\chi = 0.065(23)$. (The number in brackets indicate the standard deviation.) We see from figure 12 that this procedure is a reasonable method of extrapolation of the data for the triangular lattice, although it is not as good as for the square lattice. This is demonstrated by the magnitudes of the estimated standard deviations for the extrapolated values of χ for the square and triangular lattices (of order approximately 10^{-3} and 10^{-2}, respectively). We see from figure 12 that the main contribution to χ comes from the sublattices A and B. That is not surprising, since for the model state I, see figure 1(b), the direction of the magnetization on the sublattice C is fixed, whereas the spins on sublattices A and B are rotated towards the field direction. Indeed, we find that $\chi_{\mathrm{A,B}} = 0.0245(54)$ and $\chi_{\mathrm{C}} = 0.016(13)$ by extrapolating the susceptibilities on the different sublattices separately (see figure 12). This analysis leads again to an overall value for $\chi(=\chi_{\mathrm{A}} + \chi_{\mathrm{B}} + \chi_{\mathrm{C}})$ of $\chi = 0.065$. We can compare this result with $\chi = 0.0794$ obtained with spin-wave theory [10, 42]. (We remark that this value of χ in [42] was referred to as $\chi_{\perp}$ in this paper and furthermore that it was defined per volume.) Although the magnitudes of χ for the extrapolated CCM value and the spin-wave result agree, the difference between them is still obviously quite large. We believe that this difference might be attributed to a somewhat less reliable extrapolation (shown clearly in figure 12) than that presented for the square lattice above. However, we should note also that the spin-wave theory calculations of [42] were only ever carried out to order $1/S$. (By contrast, the spin-wave theory calculations for the square lattice were carried out to order $1/S^2$ [37].) Hence, both higher-order spin-wave results as well as higher-order CCM-LSUBm results are recommended in order to establish a more accurate figure for χ for the triangular-lattice case and, thus, to resolve this difference.

Again we mention that the zero-field uniform susceptibility $\chi(\lambda \to 0)$, together with the ground-state energy, the sublattice magnetization, the spin stiffness, and the spin-wave velocity constitute the fundamental parameter set that determines the low-energy physics of magnetic systems. Corresponding CCM results for the ground-state energy, the sublattice magnetization, the spin stiffness for the triangular-lattice Heisenberg antiferromagnet at $\lambda = 0$ can be found in [26, 30].

As for the square-lattice case above, we also present results at the LSUB4 and LSUB6 levels of approximation for the field dependence of χ in figure 13. (Note that we have LSUB8 data for χ only for small fields due to the enormous computational effort of carrying out this calculation.) Again we compare $\chi(\lambda)$ with $M/(2\lambda)$ which is often determined in experiments and also with the classical value $\chi_{\mathrm{clas}} = 1/9$ that is independent of λ.

From figure 13 it is obvious that χ and $M/2\lambda$ agree well with each other up to about $\lambda = \lambda_{\mathrm{s}}/10$ (the difference is about 7% at $\lambda = 0.45$), but deviate significantly for larger λ. As for the square lattice χ grows with λ starting from zero field up to the bottom of the plateau at λ_1. In the plateau region χ is zero indicating a finite excitation gap about the plateau ground state. Approaching the plateau from below or from above $\chi(\lambda)$ exhibits a sharp peak. Such peaks at the end of the plateau are indeed observed in experiments on an antiferromagnet on the triangular lattice, see e.g. figures 9 and 10 in [15]. Between the top of the plateau at λ_2 and the saturation at λ_{s} we find a broad region where the susceptibility is small $\chi \approx 0.1$. Approaching the saturation χ again becomes large. The oscillations seen for $\lambda \sim 3.5$ seem to be an artefact

of CCM-LSUBm approximation. However, we expect again that the amplitude of oscillation will decrease with increasing approximation level and would disappear entirely in the limit $m \to \infty$.

4. Conclusions

In this paper we describe how the coupled cluster method (CCM) may be applied in order to calculate the behaviour of quantum antiferromagnetic systems in the presence of external magnetic fields. We have determined the ground-state energy, the total lattice magnetization as well as sublattice magnetizations and the uniform susceptibility for the spin-half Heisenberg antiferromagnets on the square lattice and the triangular lattice by using the CCM to high orders of approximation. We showed that high-order CCM calculations give reasonable results for these quantities over all values of the magnetic field strength λ for both lattices. For example, the CCM result for the lattice magnetization for the square lattice compare well to QMC and spin-wave theory results for all values of the magnetic field strength. Our result for the uniform susceptibility of $\chi = 0.070$ for the square lattice is in reasonable agreement with those results of other methods (e.g., $\chi = 0.0669(7)$ via QMC). Again, we believe that even closer agreement would occur with high orders of LSUBm approximation.

CCM results presented here for the total lattice magnetization for the triangular lattice show the characteristic magnetization plateau at $M/M_s = \frac{1}{3}$ also seen in other studies [4, 7, 8, 10]. The width of this plateau was estimated by us to be given by $1.37 \lesssim \lambda \lesssim 2.15$. This result was found to be in good agreement with results of spin-wave theory [10] ($1.248 < \lambda < 2.145$) and exact diagonalizations [4, 7–9] ($1.38 < \lambda < 2.16$). Our results therefore support those of exact diagonalizations that indicate that the plateau begins at a higher value of λ than that suggested by spin-wave theory. In addition, we provide results for sublattice magnetizations M_A, M_B, and M_C evaluated on the individual sublattices A, B, and C of the triangular lattice that allows a better understanding of the magnetization process of the triangular lattice. As far as we are aware, this is the first time that results for the individual sublattice magnetizations (and angles) have been presented. Our result for the longitudinal uniform low-field susceptibility $\chi = 0.065$ compares to the result of result of spin-wave theory ($\chi = 0.0794$), i.e. there is quite a large difference between the spin-wave and the CCM result. Hence, higher-order approximations for both SWT and CCM LSUBm calculations and/or alternative approaches are recommended in order to obtain more reliable values for χ for the triangular-lattice case. The susceptibility $\chi(\lambda)$ in dependence on the magnetic field λ shows for the triangular lattice characteristic sharp peaks at the bottom and the top of the plateau which may be used as indicators in experiments for a magnetization plateau.

Acknowledgments

The present study was supported by the DFG (project Ri615/18-1). We are indebted to the research group of S Mertens for providing us access to their Tina—Beowulf-Cluster-Computer. DJJF gratefully acknowledges support for the research presented here from the European Science Foundation (Research Network Programme: Highly Frustrated Magnetism).

References

[1] Diep H T (ed) 2004 *Frustrated Spin Systems* (Singapore: World Scientific)
[2] Schollwöck U, Richter J, Farnell D J J and Bishop R F (ed) 2004 *Quantum Magnetism* (*Springer Lecture Notes in Physics* vol 645) (Berlin: Springer)
[3] Sachdev S 1999 *Quantum Phase Transitions* (Cambridge: Cambridge University Press)
Sachdev S 2004 *Quantum Magnetism* (*Springer Lecture Notes in Physics* vol 645) ed U Schollwöck, J Richter, D J J Farnell and R F Bishop (Berlin: Springer) p 381
[4] Honecker A 1999 *J. Phys.: Condens. Matter* **11** 4697
[5] Cabra D C, Grynberg M D, Honecker A and Pujol P 2001 *Condensed Matter Theories* vol 16, ed S Hernández and J W Clark (New York: Nova Science Publishers) p 17
Cabra D C, Grynberg M D, Honecker A and Pujol P 2000 arXiv:cond-mat/0010376v1
[6] Lhuillier C and Misguich G 2002 *High Magnetic Fields* (*Springer Lecture Notes in Physics* vol 595) ed C Berthier, L P Lévy and G Martinez (Berlin: Springer) p 161
[7] Richter J, Schulenburg J and Honecker A 2004 *Quantum Magnetism* (*Springer Lecture Notes in Physics* vol 645) ed U Schollwöck, J Richter, D J J Farnell and R F Bishop (Berlin: Springer) p 85
[8] Honecker A, Schulenburg J and Richter J 2004 *J. Phys.: Condens. Matter* **16** S749
[9] Nishimori H and Miyashita S 1986 *J. Phys. Soc. Japan* **55** 4448
[10] Chubukov A V and Golosov D I 1991 *J. Phys.: Condens. Matter* **3** 69
[11] Alicea J, Chubukov A V and Starykh O A 2009 *Phys. Rev. Lett.* **102** 137201
[12] Oshikawa M, Yamanaka M and Affleck I 1997 *Phys. Rev. Lett.* **78** 1984
[13] Schulenburg J and Richter J 2002 *Phys. Rev.* **65** 054420
[14] Schulenburg J, Honecker A, Schnack J, Richter J and Schmidt H-J 2002 *Phys. Rev. Lett.* **88** 167207
Richter J, Schulenburg J, Honecker A, Schnack J and Schmidt H J 2004 *J. Phys.: Condens. Matter* **16** S779
[15] Ono T, Tanaka H, Aruga Katori H, Ishikawa F, Mitamura H and Goto T 2003 *Phys. Rev.* B **67** 104431
[16] Cabra D C, Grynberg M D, Holdsworth P C W, Honecker A, Pujol P, Richter J, Schmalfuß D and Schulenburg J 2005 *Phys. Rev.* B **71** 144420
[17] Schnalle R and Schnack J 2009 *Phys. Rev.* B **79** 104419
[18] Schröder C, Nojiri H, Schnack J, Hage P, Luban M and Kögerler P 2005 *Phys. Rev. Lett.* **94** 017205
[19] Fortune N A, Hannahs S T, Yoshida Y, Sherline T E, Ono T, Tanaka H and Takano Y 2008 arXiv:0812.2077v1
[20] Kawamura H and Miyashita S 1985 *J. Phys. Soc. Japan* **54** 4530
[21] Zhitomirsky M E, Honecker A and Petrenko O A 2000 *Phys. Rev. Lett.* **85** 3269
Zhitomirsky M E 2002 *Phys. Rev. Lett.* **88** 057204
[22] Moliner M, Cabra D C, Honecker A, Pujol P and Stauffer F 2008 arXiv:0809.5249
[23] Roger M and Hetherington J H 1990 *Phys. Rev.* B **41** 200
Roger M and Hetherington J H 1990 *Europhys. Lett.* **11** 255
[24] Bishop R F, Parkinson J B and Xian Y 1991 *Phys. Rev.* B **44** 9425
[25] Xian Y 1994 *J. Phys.: Condens. Matter* **6** 5965

[26] Zeng C, Farnell D J J and Bishop R F 1998 *J. Stat. Phys.* **90** 327
[27] Bishop R F, Farnell D J J, Krüger S E, Parkinson J B, Richter J and Zeng C 2000 *J. Phys.: Condens. Matter* **12** 7601
[28] Farnell D J J, Gernoth K A and Bishop R F 2002 *J. Stat. Phys.* **108** 401
[29] Farnell D J J, Schulenberg J, Richter J and Gernoth K A 2005 *Phys. Rev.* B **72** 172408
[30] Krüger S, Darradi R, Richter J and Farnell D J J 2006 *Phys. Rev.* B **73** 094404
[31] Darradi R, Derzhko O, Zinke R, Schulenburg J, Krüger S E and Richter J 2008 *Phys. Rev.* B **78** 214415
Richter J, Darradi R, Zinke R and Bishop R F 2007 *Int. J. Mod. Phys.* B **21** 2273
[32] Farnell D J J, Richter J, Zinke R and Bishop R F 2009 *J. Stat. Phys.* **135** 175
[33] http://www-e.uni-magdeburg.de/jschulen/ccm/index.html
[34] Kubo R 1952 *Phys. Rev.* **87** 568
Oguchi T 1960 *Phys. Rev.* **117** 117
[35] Runge K J 1992 *Phys. Rev.* B **45** 12292
[36] Weihong Z, Oitmaa J and Hamer C J 1991 *Phys. Rev.* B **43** 8321
[37] Hamer C J, Weihong Z and Arndt P 1992 *Phys. Rev.* B **46** 6276
[38] Zhitomirsky M and Nikuni T 1998 *Phys. Rev.* B **57** 5013
[39] Lüscher A and Läuchli A M 2008 arXiv:0812.3420
[40] Chernyshev A L and Zhitomirsky M E 2009 arXiv:0902.4455
[41] Manousakis E 1991 *Rev. Mod. Phys.* **63** 1
[42] Chubukov A V, Sachdev S and Senthil T 1994 *J. Phys.: Condens. Matter* **6** 8891
[43] Trumper A E, Capriotti L and Sorella S 2000 *Phys. Rev.* B **61** 11529
[44] Zheludev A, Maslov S, Shirane G, Sasago Y, Koide N and Uchinokura K 1997 *Phys. Rev. Lett.* **78** 4857
[45] Schröder C, Prozorov R, Kögerler P, Vannette M D, Fang X, Luban M, Matsuo A, Kindo K, Müller A and Todea A M 2008 *Phys. Rev.* B **77** 224409
[46] Engelhardt L, Martin C, Prozorov R, Luban M, Timco G A and Winpenny R E P 2009 *Phys. Rev.* B **79** 014404
[47] Villain J, Bidaux R, Carton J P and Conte R 1980 *J. Physique* **41** 1263
[48] Shender E F 1982 *Zh. Eksp. Teor. Fiz.* **83** 326
Shender E F 1982 *Sov. Phys.—JETP* **56** 178 (Engl. Transl.)
[49] Kubo K and Kishi T 1990 *J. Phys. Soc. Japan* **60** 567